

Photocreated metastable states in polysilanes

Kyozauro Takeda, Kenji Shiraishi, and Michiya Fujiki
NTT Basic Research Laboratories, Morinosato, Kanagawa 243-01, Japan

Michio Kondo* and Kazuo Morigaki†
Institute for Solid State Physics, University of Tokyo, Roppongi, Tokyo 106, Japan

(Received 7 March 1994)

Photocreated metastable states in organopolysilane (PSi) solids are observed using the electron-spin-resonance (ESR) technique. Two types of light-induced ESR (LESR) spectra are found depending on the excitation photon energy. These two types of LESR centers are annihilated by thermal annealing. Based on a first-principle electronic calculation, the origins of these LESR centers have been discussed. The lowest photoexcitation (~ 3.5 eV) in PSi induces the Si skeleton stretching forces, which creates a weak bond (WB) in several places of the Si skeleton. Electronically, this WB acts as a self-trapping center for the photoexcited σ electron. The other higher photoexcitation (over 4.8 eV) causes side-pendant dissociation, which creates a dangling bond (DB) and causes the localized midgap state. The four lines found in the higher-energy excitation are considered to arise from hyperfine interaction between this DB electron and a sodium impurity nucleus.

I. INTRODUCTION

Polysilane (PSi) is a chainlike polymer, whose backbone is formed by Si atoms. Many kinds of organic substituents affect the PSi material system.¹ Recently, much attention has been paid to the optical properties of PSi, and studies have revealed ultraviolet absorption,² photoconduction,³⁻⁵ photoluminescence,⁶ two-photon absorption,⁷ excitonic states,⁸ and triplet states.⁹

Since highly hydrogenated amorphous silicons (α -Si:H) contain Si chain forms,¹⁰ several similarities between PSi and α -Si:H have been reported.^{10,11} There are also apparent differences between these two materials. The most interesting one is that mobile holes have been observed in PSi photoconduction,³⁻⁵ while holes in α -Si:H tend to be self-trapped.^{12,13}

The purpose of this paper is to observe photocreated metastable centers in solid-state PSi by using the light-induced electron-spin-resonance (LESR) technique, and to discuss those origins theoretically based on a first-principle local-density-functional (LDF) calculation.¹⁴

There have been several ESR experiments with PSi performed in the solution state. By using these PSi solutions, photodegradation and reactive intermediates in PSi synthesis have been investigated intensively by several groups.¹⁵⁻¹⁷ Although some persistent silyl radicals and silylenes have been found, those investigations were limited to those in PSi solutions. For solid PSi, no ESR experiments have yet been reported. Recently, Benfield *et al.*¹⁸ studied the ESR spectrum for solid residues in PSi synthesis (not PSi itself but the blue precipitates in PSi synthesis). They found that sodium impurities play an important role in the blue color center in PSi synthesis, but did not report the electronic structure of photoexcited solid PSi. Here we focus on whether photocreated metastable states are a self-trapping center for

electrons, and on how the sodium impurities acts in the photoexcited solid PSi.

PSi stands at the crossing point of crystal Si and α -Si:H and also other Si materials, e.g., porous Si. A knowledge of the photocreated metastable states in PSi will help in understanding those Si skeleton materials.

II. EXPERIMENTS AND RESULTS

Three kinds of organopolysilanes, methylpropylpolysilane, methylphenylpolysilane, and dihexylpolysilane, were used for the ESR measurements. All samples were prepared by a conventional Wurtz-type coupling reaction in dry toluene in an argon atmosphere using a sodium lump. The corresponding starting monomers are methyl(*n*-propyl)dichlorosilane, methylphenyldichlorosilane, and di(*n*-hexyl)dichlorosilane. After 2-3 h at about 110°C, the reaction mixture was cooled to room temperature and passed through a 0.45- μ m poly(tetrafluorethylene) filter under argon gas pressure. The filtrate was poured into *iso*-propanol and the resulting precipitate was collected by centrifugation and dried at 60°C *in vacuo* overnight. The yield of all polymers ranged from 10 to 20%. The weight averaged molecular weight of polymers (M_w) and polydispersity (D), which are determined based on a calibration with polystyrene standards, are as follows: for methylpropylpolysilane, $M_w=10\,500$, $D=2.0$; for methylphenylpolysilane, $M_w=9700$, $D=1.8$; and for dihexylpolysilane, $M_w=20\,200$, $D=2.2$.

The polymer characterization was also carried out by high-resolution NMR measurements. For solution-phase PSi in deuterated chloroform, ²⁹Si-NMR spectra were obtained by a Varian Unity-300 NMR spectrometer at 59.59 MHz with the gated decoupling pulse technique for excluding the nuclear Overhauser effect. ²⁹Si-NMR spec-

tra for solid-phase PSi and other insoluble Si-skeleton samples were recorded by a Varian Unity-400 NMR spectrometer at 79.46 MHz with the cross-polarization (CP)-magic-angle spinning (MAS) technique.

ESR measurements were carried out at the X-band region using a JEOL JESFE1X. Two different lamps (a 500-W high-pressure Xe arc lamp with an UV-D1B filter and a 150-W low-pressure Hg lamp without optical filters) were used as exciting light sources. The corresponding wavelengths are ~ 350 (lower-energy excitation) and 254 nm (higher-energy excitation), respectively. The Hg irradiation also includes light of the wavelength 185 nm. These light irradiations were performed at 10 K and light-induced ESR (LESR) signals were observed at the same temperature.

Figure 1 shows the LESR spectrum for methylpropylpolysilane with lower-energy excitation. The g value of this center is 2.0044, and the width (peak-to-peak separation, ΔH_{pp}) is 30 G.¹⁹ The estimated spin density is about 2×10^{15} spins/g.²⁰ Even after the illumination was turned off, this ESR center was frozen at 10 K, but was completely annihilated by the thermal annealing at room temperature (RT). The important point is that the LESR centers are not found irradiated at RT. This evidence is apparently different from that for solution PSi, in which the RT irradiation causes LESR.¹⁵⁻¹⁷

A similar LESR signal was also observed in methylphenylpolysilane (Fig. 2). Except for a slight narrowing in the signal band-width, the numerical values of g and ΔH_{pp} are same as those of methylpropylpolysilane. Dihexylpolysilane shows a slightly different LESR spectrum of $g=2.0026$ and $\Delta H_{pp}=10$ G. The long lifetime and the complete annihilation by thermal annealing are common characteristics in the present PSi solids. Since the observed LESR signals are independent of the kinds of the side chains, it can be concluded that these LESR signals originate from the paramagnetic state of unpaired electrons at Si skeleton atoms of PSi.

Figure 3 shows the LESR spectrum for dihexylpolysi-

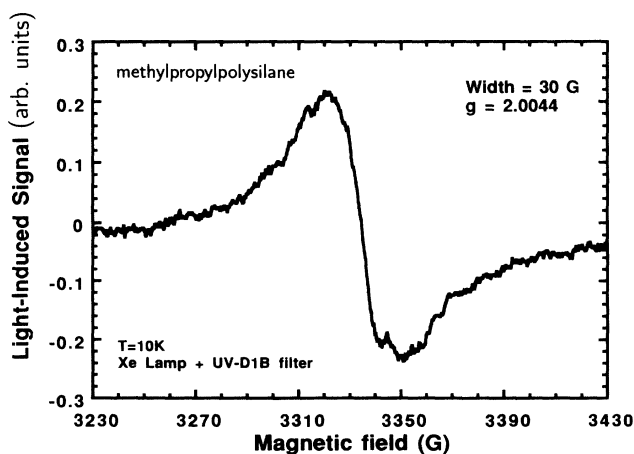


FIG. 1. Light-induced ESR spectrum for lower-energy excitation in methylpropylpolysilane. The measurement was done at 10 K, and microwave power was 0.1 mW. The light source was a Xe lamp with a UV-D1B filter.

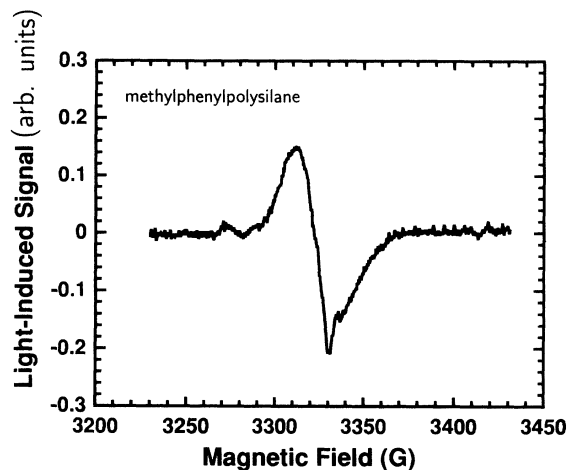


FIG. 2. Light-induced ESR spectrum for lower-energy excitation in methylphenylpolysilane. The measurement was done at 10 K, and microwave power was 0.1 mW. The light source was a Xe lamp with a UV-D1B filter.

lane under higher-energy excitation. An additional structure can be clearly observed in this spectrum.²¹ The characteristic feature is that this additional structure almost disappears after thermal annealing at over 50 K (Fig. 4), and the remaining spectrum resembles those spectra observed under the lower-energy excitation: In dihexylpolysilane, for instance, the sample annealed at 50 K shows a structureless signal with $g=2.0047$ and $\Delta H_{pp}=25$ G.

III. THEORETICAL CALCULATION

In order to discuss the origins of the above two types of LESR centers, we theoretically investigate which metastable states are possible to create by photoexcitations, and how band-edge states are changed when the corresponding metastable state is created. The theoretical cal-

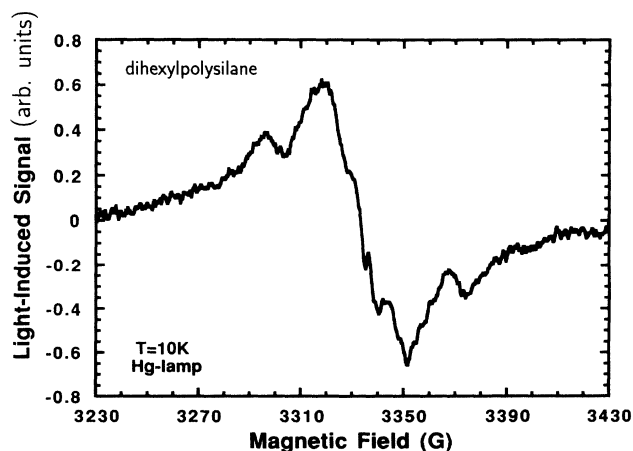


FIG. 3. Light-induced ESR spectrum for higher-energy excitation in dihexylpolysilane. The measurement was done at 10 K, and microwave power was 0.1 mW. The light source was a Hg lamp without optical filter.

calculations were performed using the first-principles local-density-functional (LDF) method.^{22,23} The norm-conserving pseudopotential^{24,25} was used, in which core basis functions are neglected in the calculation. The exchange-correlation energy is approximated by the functional form of Ceperley and Alder's²⁶ potential parametrized by Perdew and Zunger.²⁷ Details of the calculation have been reported in our previous works.^{14,28}

LDF band calculations^{14,29} reveal the electronic structure of PSi.³⁰ At the band-edge states (Fig. 5), σ electrons of the skeleton Si atoms are well delocalized along the skeleton chain axis (σ conjugation).³¹ The highest occupied valence-band (HOVB) state is formed of the $p\sigma$ bonding state between the skeleton Si $3p_x$ atomic orbitals (AO's). The lowest unoccupied conduction-band (LUCB) state is formed of the $sp\sigma^*$ antibonding state between the skeleton Si $2s$ and $3p_y$ AO's.

A. Optically selective scissoring

Hellmann-Feynman forces working at each atom are calculated by the gradient method of the total energy, when the hypothetical electron excitations from the i th valence band (VB) to the j th conduction band (CB) are considered. The hypothetical electron excitations con-

TABLE I. Calculated Hellmann-Feynman stretching forces working on Si-Si/Si-H bonds. The plus sign means the stretching direction, and the unit of forces is 10^{-2} Ry/a.u. The calculated energy gaps (in eV) are also given in parentheses.

State	$sp\sigma^*$	quasi- π^*
$p\sigma$	3.49/-0.87 (3.89)	5.42/-0.39 (5.42)
quasi- π	-5.37/2.01 (6.10)	-7.63/3.37 (7.59)

sidered are the following four combinations from $p\sigma$ or quasi- π VB states to $sp\sigma^*$ or quasi- π^* CB states. The calculated forces are summarized in Table I. The electron excitations from the $p\sigma$ band cause the stretching force on the Si-Si skeleton bond. However, these excitations do not induce dissociating forces on the Si-H pendant bond. Such a dissociating force is caused by the electron excitation from the quasi- π band.

The optical selection rule limits some of the above electron excitations. According to the symmetry of the transplanar form (Table II), the optical electron excitation from $p\sigma$ to quasi- π^* bands is ruled out. Therefore, in PSi, the Si skeleton-bond stretching force is induced by only the lowest optical excitation, while other high optical excitations induce the dissociating forces at the

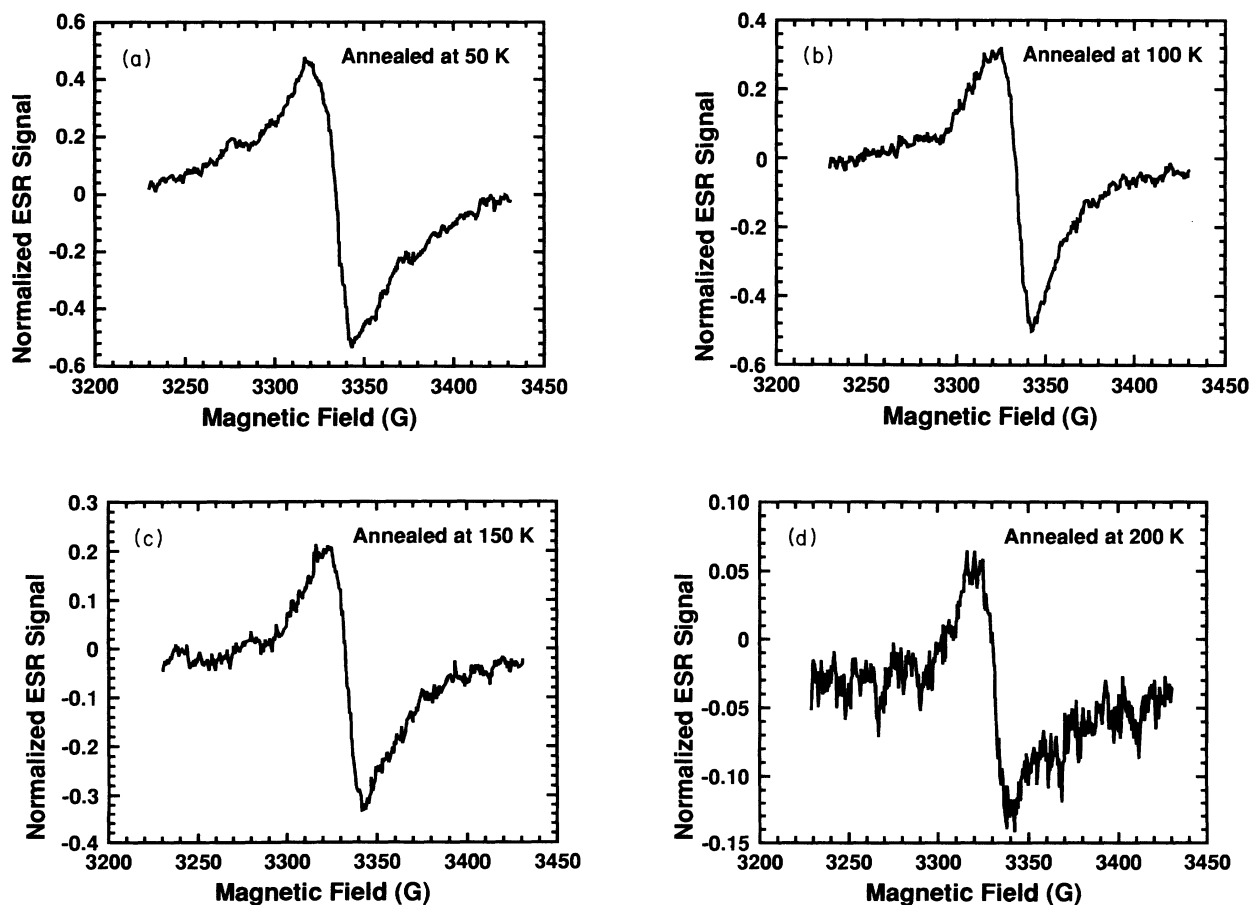


FIG. 4. ESR spectrum for annealed dihexylpolysilane. The sample illuminated by the Hg lamp without optical filter at 10 K (Fig. 2) was annealed at temperatures of 50 (a), 100 (b), 150 (c), and 200 K (d) for 30 min. After each thermal annealing, the sample was recooled at 10 K for ESR measurement. Signal values are normalized to that in Fig. 2.

TABLE II. Symmetric properties of the orbital for the optical excitation and induced metastable states expected in the corresponding optical excitation. A transplanar structure is assumed, because PSi chains tend to show this form at low temperature.

State	$sp\sigma^*(B_{3u})$	quasi- $\pi^*(B_{2u})$
$p\sigma(B_{2g})$	$B_{1u}(x)/WB$	$A_u(\text{forbidden})$
quasi- $\pi(B_{1g})$	$B_{2u}(z)/DB$	$B_{3u}(y)/DB$

skeleton-pendant bond. The former forces creates a weak bond (WB)-type metastable state in the Si skeleton, while a dangling bond (DB)-type metastable state is expected to be created at the pendant position by the latter force. Thus, by tuning the photon energy of the irradiation, we can create different kinds of metastable states in PSi (optically selective bond scissoring). The corresponding electronic structures of these WB's and DB's are discussed in the following.

B. Weak bond

Here a simple WB is considered by stretching a part of the uniform Si skeleton bond in order to investigate how

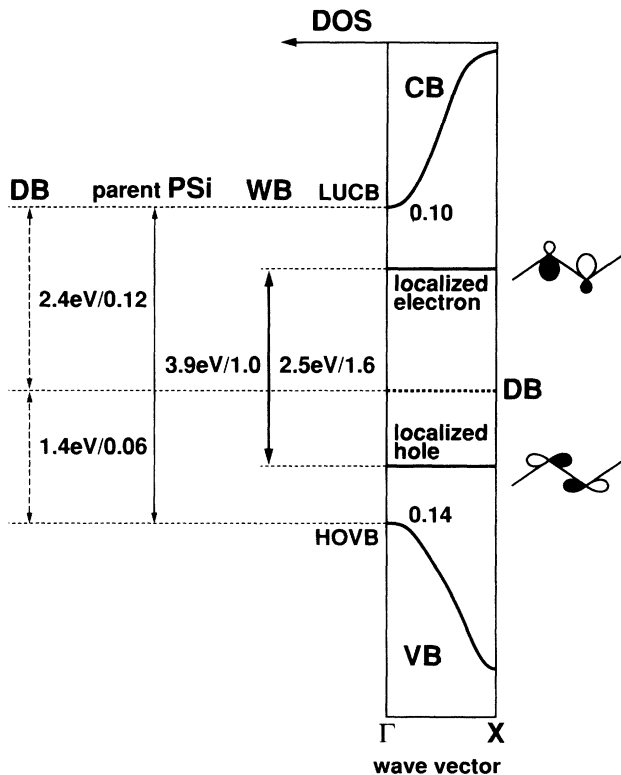


FIG. 5. Calculated electronic structure of PSi near the Fermi level. For simplicity, only two E - k dispersion curves of the lowest CB and highest VB are shown for parent PSi. The localized electron-tail and hole-tail states caused by WB are also represented. The broken line indicates the singly occupied localized level caused by DB. The arrows are values of the energy gaps, and the numerical value at each arrow is the optical transition matrix element normalized to that of the parent PSi. Orbital characters and values of effective masses at HOVB and LUCB are also shown in figure.

the WB changes the band-edge electronic structure. A stretching length of 0.65 Å, a half of the Van der Waals radii for Si, is assumed here. This value is amount to 27% of the optimized Si-Si skeleton-bond length of the parent PSi, and corresponds to the remarkably strong WB, compared with those of three typical valence WB's in a -Si (17–45%). Calculations were performed using a supercell approach containing four Si atoms and eight H atoms. By comparing a larger unit cell including six Si atoms and 12 H atoms with the result, it was found that this supercell is large enough to lead to a discussion of the localized states.

Electronically, the band-edge states are changed remarkably by the WB as follows: The local Si skeleton-bond stretching weakens the $p\sigma$ bonding character of the HOVB state and destabilizes this state. Therefore, the original HOVB state energetically shifts upwards and forms a hole-tail state with localizing around the WB site. Conversely, a reduction in the $sp\sigma^*$ antibonding character stabilizes the LUCB state energetically to shift the original LUCB state downwards, and an electron-tail state is formed. Thus an appearance of WB's cuts the σ conjugation of the band-edge states and creates the tail states (Fig. 5). These tail states effectively reduce the band gap (E_g). A 35% E_g reduction from that of the parent PSi is found when a larger WB with 27% stretching is introduced.

Figures 6(a) and 6(b) show the charge-density (CD) distribution of holes and electrons at each localized tail state, respectively. Holes localize at the position of the

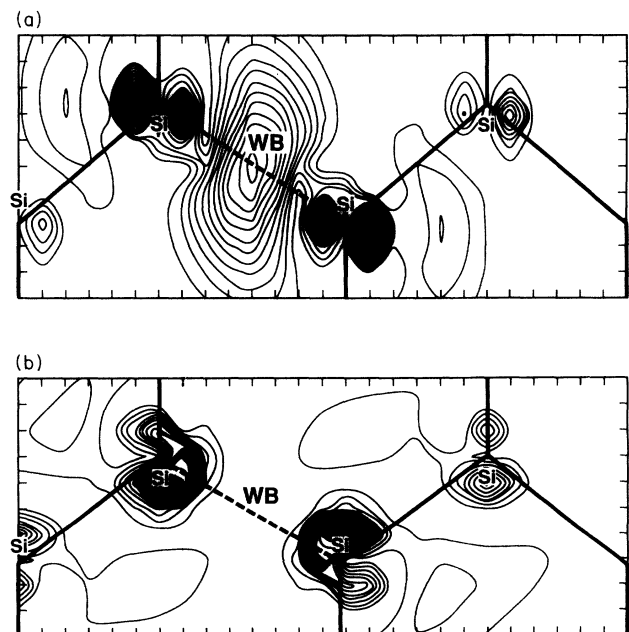


FIG. 6. Contour of density profiles of (a) the tail hole and (b) the tail electron around the WB indicated by the broken line. In the figure, the contour plot on the skeleton plane is shown from 0 to 90 (a) and to 120 (b) with an interval of 5.0 (a.u.). The horizontal interval is 0.324 Å and the vertical interval is 0.328 Å.

WB center [Fig. 6(a)]. The tail-state electrons tend to localize at two Si atoms on this WB [Fig. 6(b)]. However, one should find that these tail electrons and holes maintain original orbital symmetries of the delocalized band-edge states. Therefore, an optical transition between them is possible. Moreover, a large optical transition matrix element is expected between these two tail states because of their spatial localizations. The calculated value is 1.6 times larger than that of the parent PSi. Thus WB's, created by stretching the Si skeleton bond, act as "radiative centers" in PSi, if the excited electron hole does not separate spatially.

C. Dangling bond

When a side-pendant group (a H atom in the present work) is dissociated from PSi, a strongly localized state appears in the midgap position of the original E_g (Fig. 5). Electronically, the dissociation of the side groups from the PSi system decomposes the quasi- π states, and then reverts it to its original levels of Si atom,³¹ because these bands are formed by the skeleton-pendant interaction between Si $3p_z$ and H $1s$ AO's. Thus the localized level appearing in the midgap position of E_g is the Si dangling-bond (DB) level, which is singly occupied.

The electron localization at this DB level, however, is oriented toward the out-of-skeleton plane direction (Fig. 7). Therefore, the optical transition matrix elements between this DB level and the band-edge state (HOVB or LUCB) are very weak. They are only 6% (between DB and HOVB) and 12% (between DB and LUCB) of that in the saturated PSi (between HOVB and LUCB). Thus the dangling bond created by the pendant group dissociation play the role of a "nonradiative" center in PSi. It is also characteristic that the DB level formation hardly changes the band-edge states. The reason is that these band-edge states are formed of the skeleton in-plane σ electrons orthogonal to that of Si-DB electrons.

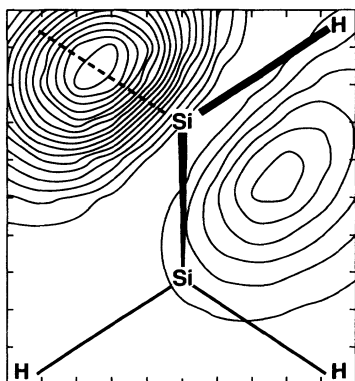


FIG. 7. Contour of density profiles of the DB state. The contour plane is defined by one Si atom and two H atoms, one of which is dissociated, and the plane is viewed from the skeleton axis. The broken line indicates the corresponding broken Si-H bond. The three lower atoms of H-Si-H are out of this plane. In the figure, the contour is shown from 0 to 85.0 with an interval of 5.0 (a.u.). The horizontal interval is 0.235 Å and the vertical interval is 0.322 Å.

D. Paramagnetic character of WB and DB

The observation of the paramagnetic electron-spin-resonance (ESR) signal from the DB can naturally be expected, because this state is singly occupied by an electron. On the contrary, most of the tail electrons and tail holes of the WB seem to recombine, and that metastable immediately stabilizes into the ground (singlet) state, because of the large values of the optical transition matrix element. However, there is also a possibility that some of those excited electron-hole pairs survive from the recombination and form paramagnetic states ($S = \frac{1}{2}$). This possibility originates from the spatial separation of the excited tail electrons and tail holes.

When the WB is induced along the Si skeleton, band-tail states appear symmetrically around the Fermi energy; e.g., these band-tail states are settled in the band gap about 0.7 eV far from the original HOVB or LUCB states for the present large WB with 27% stretching. Therefore, the trapping depths are equivalent for tail electrons and tail holes. However, the itinerancy of tail-edge states is slightly different between electrons and holes. The calculated transfer energy of the tail electron is 1.5 times as small as that of the tail hole. Thus tail-edge electrons tend to be trapped effectively but tail-edge holes tend to be itinerant, and some of photogenerated electron-hole pairs are able to separate spatially.³² Therefore, the WB as well as the DB forms a possible paramagnetic state, which can be observed by ESR experiments.

In the present theory, we assume a transplanar zigzag backbone in PSi chains. Of course, actual PSi chains having organic side chains are known to form random and helical backbones rather than transplanar and uniform backbones. Therefore, the application of the above results should be limited. Dihexylpolysilane, however, is an exception, which is known to form a transplanar backbone at low temperature, and might be a good applicable example. Moreover, present theoretical results are applicable to crude discussions about other PSi chains, when these chains partially include transplanar backbones.

IV. DISCUSSION

A. LESR by lower-energy excitation

Based on the theoretical results above, let us first discuss the origin of the LESR center by lower-energy excitation. The energy of the present lower excitation corresponds to that of the σ - σ^* transition. Theoretically, this optical excitation induces the Si-Si bond-stretching force and forms the WB's. As mentioned in Sec. III, these WB's work to become a trapping center of the photoexcited σ electrons, and have the potential to become a paramagnetic state. The long lifetime of the observed LESR signal at 10 K and the annihilation of the signal by the thermal annealing are consistent with our theoretical results that some of those excited σ electrons and σ holes are trapped with a spatial separation by the difference between their itinerancies sufficiently to suppress their recombinations. Therefore, it can be concluded that the lower-energy excited LESR is caused by the paramagnetic state of these σ electrons self-trapped at WBs.³³ The

observed g value (2.0044) is also closer to that of the tail electron (2.004) than that of the tail hole (2.01) in a -Si:H.

The observation of LESR by the lowest optical excitation has an important meaning. At the present state, the lowest optical transition in P*Si* is accepted as being caused by a one-dimensional (1D) singlet exciton whose lattice deformation is small.⁸ The observation of this LESR should, however, change the previous interpretation slightly, because the singlet state is inactive by ESR measurements. The 1D singlet exciton model is based on the assumption that the P*Si* skeleton is fully extended or has a uniform Si skeleton rod.⁸ The real P*Si*,^{34,35} however, is a model 1D *disordered system* rather than a 1D *uniform system*; Si skeleton atoms are segmented by some disorderings and distorted bonds, e.g., kinks.³⁶ These rod-broken points have a potential to become WB centers and form a paramagnetic metastable state when the lowest amount of optical absorption occurs. Thus, although most of the lowest absorption occurs at these extended rod parts through the 1D singlet excitons which can delocalize within these extended rod parts, one should pay attention to the role of the actual rod-broken points.

The metastability of these disorderings strongly depends on whether P*Si* is in solid or in-solution phase. Since P*Si* molecules in solution or glassy solution phases stand freely, these disorderings of rod-broken points easily relax into their ground states. Conversely, the bond distortions and rod-broken points are conserved in solid P*Si*. This feature is confirmed by ²⁹Si NMR spectroscopy. In Fig. 8, we show the high-resolution solid-state ²⁹Si-NMR spectrum of methylphenylpolysilane used in the present experiments both in solid and in-solution phases, comparing them with those of other Si skeleton materials. The NMR spectra are measured by the CP/MAS technique. A shoulder band in the down-field region of the main Si NMR signal is found in solid P*Si* but not in-solution P*Si*. This broad signal is caused by the nonuniformity and the distortion in Si-Si bonds. A similar broadness in the NMR signal is found in a -Si,

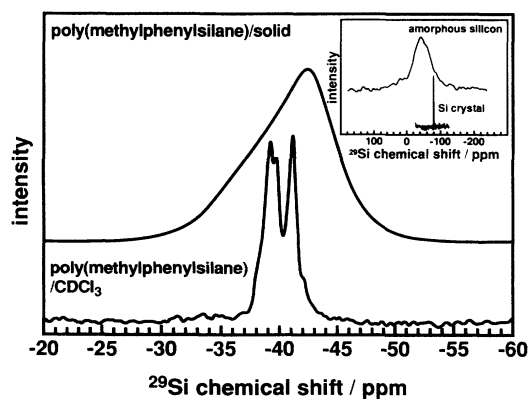


FIG. 8. Comparison of high-resolution solid-state ²⁹Si NMR spectra of methylphenylpolysilane in both solid-state and in solution phases. The spectra are measured by the cross-polarization-magic-angle spinning technique. In the figure, solid-state ²⁹Si NMR spectra of c -Si and a -Si are also shown for comparison.

which includes many distorted Si-Si bonds. Thus solid P*Si* chains contain more distorted Si-Si bonds than solution P*Si* chains do.

These distorted Si-Si bonds originally form a diamagnetic state. When the lowest optical transition occurs, some of these disorderings can change into a paramagnetic state via the mechanism discussed in Sec. III. However, in the solid-state phase, the RT thermal energy easily anneals the photo created paramagnetic state and puts it back into the diamagnetic ground state, because of its metastability. At low temperature, these photocreated metastable states are frozen and can be observed. This is the reason why we cannot find the LESR signal in solid-state P*Si* irradiated at RT. Conversely, bonds once scissored by the photoabsorption can live in solution phase even at RT. McKinley *et al.* observed these bond scissorings as persistent radicals through LESR measurement in the P*Si* solution at RT.¹⁷

Based on the present spin densities,²⁰ such LESR centers are distributed in each Si catenation of 10–100 atoms. This estimation is consistent with the results of absorption saturation measurements by Thorne *et al.*,³⁷ However, it is unclear why no contribution from the surviving holes was found in the present experiments. The broad width of the ESR signals may include contributions from both electrons and holes. However, it is possible that the corresponding integrated LESR signal is fitted by a single Lorentzian. This is the most significant difference from a -Si:H.¹²

B. LESR by higher-energy excitation

In the present higher-energy excitation, the Hg lamp irradiation causes optical transitions such as those summarized in Table II, in addition to σ - σ^* electron excitation by the Xe lamp. Theoretically, these additional electron transitions induce the dissociating force working at the pendant bonds and form DB's. The spatial extension of the DB wave function (Fig. 7) is expected to proceed out of the skeleton, and is apparently different from those in the WB states [Figs. 6(a) and 6(b)]. The experimental difference in LESR signals caused by lower- and higher-energy excitations is the additional structure found in the higher-energy excited LESR. Focusing on the difference in the spatial extension of WB and DB states, is it possible to understand the origin of the additional ESR structure in terms of the hyperfine interaction with ²⁹Si nuclei?

Here we calculated the isotropic hyperfine interactions a between the unpaired electron in these two possible metastable states and ²⁹Si nuclei at the various positions of the skeleton. The value of a due to ²⁹Si at site R_n is expressed in gauss unit as follows:^{38,39}

$$a = 317 |\Psi_i(R_n)|^2 .$$

Here $\Psi_i(R_n)$ is the wave function of the unpaired electron or hole of the metastable state of $i = \text{WB}$ or DB , respectively. As we used the pseudopotential and the Gaussian-type pseudo-wave-function for $\Psi_i(R_n)$, the values of $\Psi_i(R_n)$ are estimated by the interpolating fitting technique in the small region including the R_n site. Figure 9 shows calculated ²⁹Si hfc constants, when two types

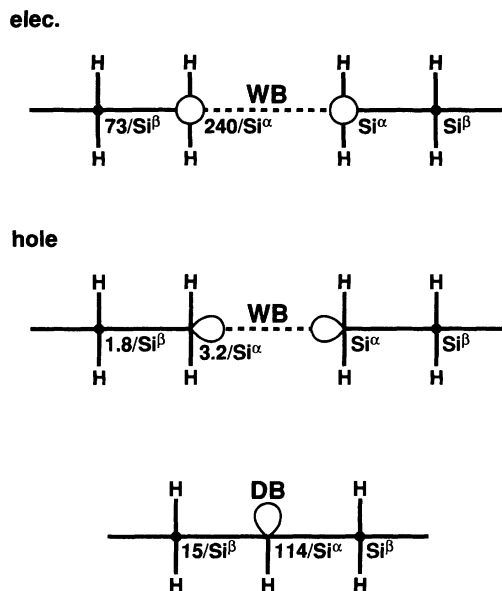


FIG. 9. Values of calculated ^{29}Si hfc constants for WB and DB in units of G. Si^α atoms in WB are positioned to place the WB (broken line), and Si^β atoms at the neighbor sites of Si^α atoms. The Si^α atom in DB has DB at its side-chain position, and Si^β atoms are positioned at Si^α 's neighboring sites.

of metastable states are created.

In the case of WB formation (Fig. 6), tail-edge electrons [Fig. 6(b)] tend to localize on both sides of two Si atoms (α position) on the WB. Electronically, these metastable states are composed of Si 3s AO's. Therefore, a larger hfc constant would be expected. Conversely, the hfc value for holes of the WB tail edge is very small, because this state is formed mainly of the Si 3p AO's [Fig. 6 (a)]. An intermediate hfc constant would be expected from the Si^α atom of DB, because the corresponding spin density localizes toward the out-of-plane position. This out-of-plane localization for the unpaired electron at the DB level steeply reduces the values of hfc constants caused by second-neighbor Si atoms (Si^β).

These characteristic features of ^{29}Si hfc could not be found in the higher-energy excited LESR signals or in the lower-energy excited LESR signals, although the calculated hfc value for DB seems to be comparable to that found by Mckinley *et al.*¹⁷ Thus we cannot confirm directly whether the DB-type metastable state is created by higher-energy excitation. However, we found another fine structure through higher-energy excitation by the sample annealing procedure.

C. Annealing effects

Samples illuminated by Hg lamp at 10 K were annealed at several temperatures of 50, 100, 150, and 200 K for 30 min. After each annealing, the samples were recooled at 10 K to measure the ESR signal. In the following, we report the results for dihexylpolysilane. The others for methylpropylpolysilane and methylphenylpolysilane will be reported elsewhere, including a detailed discussion of the annealing effects.

Figures 4(a)–4(d) show the observed ESR signals with

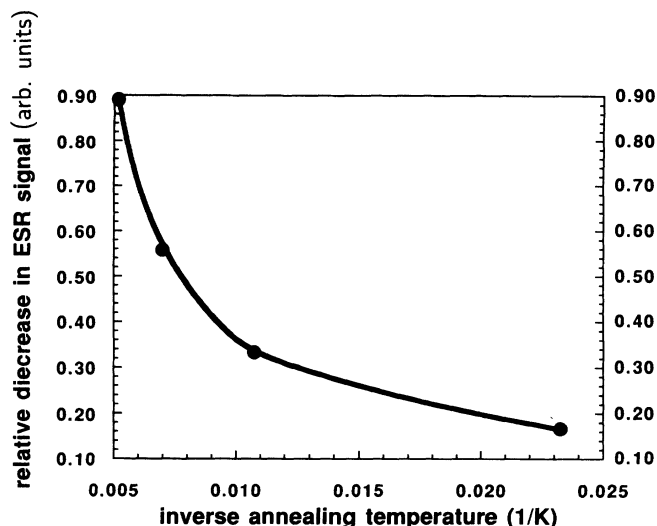


FIG. 10. Change in ESR signal intensity of dihexylpolysilane with varying annealing temperatures. Signal intensities are estimated from the peak-to-peak value of ESR signals at corresponding annealing temperatures, and values relative to that at 10 K are shown.

varying annealing temperatures. The additional ESR structure caused by the higher-energy excitation almost disappears when the sample is annealed at 50 K. When the annealing temperature is higher than 100 K, the broad component in the ESR signal disappears. It is also characteristic that the intensity of the annealed ESR signals weakens with increasing annealing temperature.

When the effective quenching of the paramagnetic spins is assumed to occur via the thermal activating process, the Arrhenius-type curve is expected in the relation between the paramagnetic spin density and the annealing temperature. However, an apparent discrepancy from this Arrhenius (linear) relation is found in Fig. 10, in which the decrease of the ESR signal intensity is plotted with inverse values of the annealing temperature. This discrepancy means that quenching of the paramagnetic

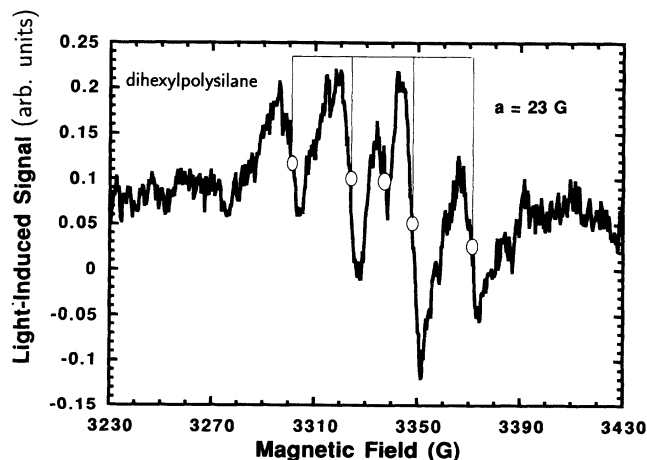


FIG. 11. Difference in the ESR spectrum of dihexylpolysilane between the higher-energy-excited LESR and the signal annealed at 50 K. Open circles show the center field for each line. The four equally separated spectra are designated by their lines in the figure. The separation is about 23 G.

spins by thermal annealing does not occur via a simple activating process.

The complexity of the thermal quenching is also confirmed by Figs. 11 and 12(a)–12(c) in which the subtracted ESR spectrums are shown. Figure 11 shows the difference in ESR signals between the higher-energy ex-

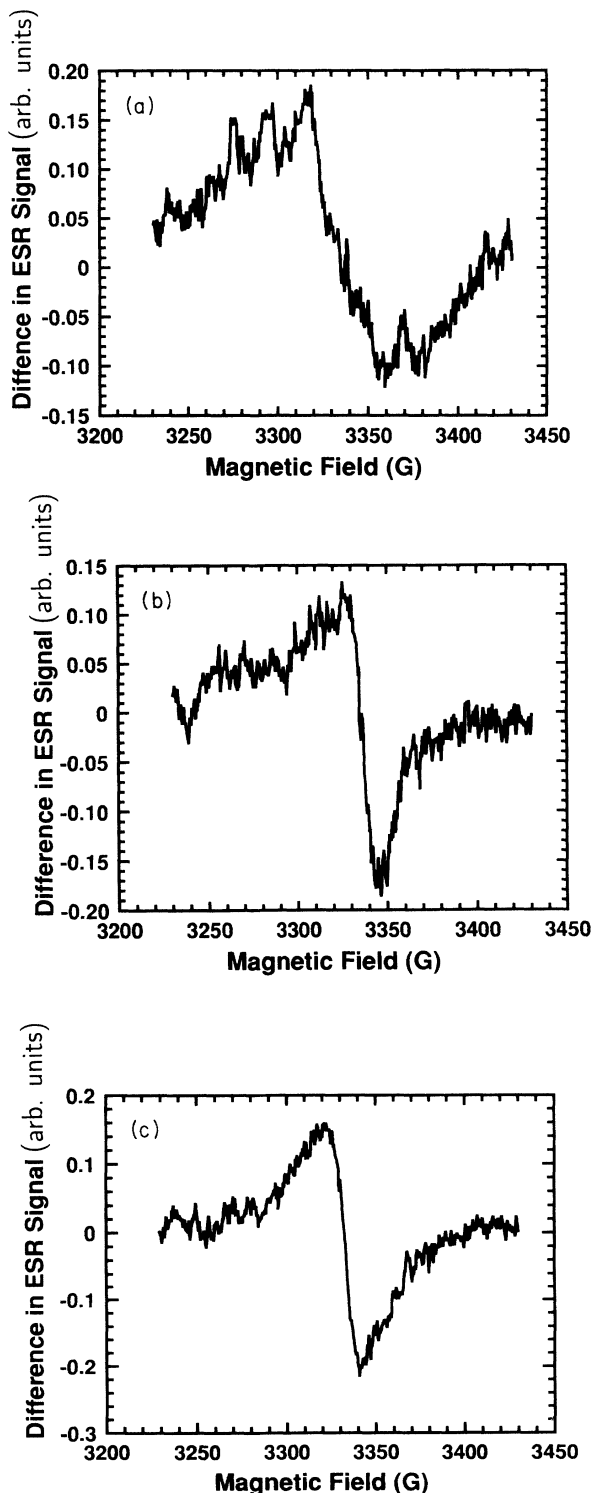


FIG. 12. Difference in the ESR spectrum of dihexylpolysilane between the signals annealed at 50 and 100 K (a), those annealed at 100 and 150 K (b), and those annealed at 150 and 200 K (c).

cited LESR signal and the signal annealed at 50 K. Figures 12(a)–12(c) show the difference in ESR signals between those annealed at 50 and 100 K, those annealed at 100 and 150 K, and those annealed at 150 and 200 K, respectively. These signals give the ESR component quenched at the corresponding annealing temperature.

Four distinct lines are found in Fig. 11, and they separate equally (hyperfine quartet). The g value of the center spectrum is 2.0026. This hyperfine quartet is the disappearing component caused by thermal annealing at 50 K. The thermal annealing at 100 K quenches the broad component of the LESR signal [Fig. 12(a)], which is different from the quenched components caused by 150- and 200-K annealings [Figs. 12(b) and 12(c)]. Thus each annealing process quenches a different paramagnetic center.

Purifying the samples revealed that the hyperfine quartet strongly correlates with the sodium (Na) impurity content in the sample. The flame spectrochemical analysis showed a 1/200 reduction of sodium impurities by the reduced-pressure filtration with 0.45- μm pores. In these purified samples, the hyperfine quartet was significantly reduced. Considering that the nucleus spin of Na is $I = \frac{3}{2}$ and its natural abundance is 100%, these four lines could be identified with a hyperfine quartet caused by interchain sodium impurities.⁴⁰

The DB is a possible candidate to interact with these Na impurities. The reasons are as follows: Na impurities should be located at the interchain sites, because PSi samples are synthesized by the dechlorine reaction when mixed with small fragments of metallic Na. Therefore, Na impurities can interact with the DB, in which an unpaired electron is localized toward the out-of-skeleton plane, i.e., the interchain direction.

The isotropic hyperfine constant of atomic Na is 224 G.⁴¹ The present one is estimated to be ~ 23 G, which is $\frac{1}{10}$ of the atomic value. This reduction is qualitatively understandable because of the strong anisotropy of the localized DB state.²⁸ The distinct hyperfine quartet also suggests the existence of a specific metastable position of sodium impurities. One possible position might be an interstitial back-bond position, which is theoretically predicted for the hydrogen in PSi.²⁸

V. CONCLUSION

We observed photocreated metastable centers in solid-state PSi by using the LESR technique. Based on a first-principle electronic calculation, the following are concluded.

(i) The lower optical excitation (Xe lamp) in solid PSi creates the paramagnetic centers which are observed to be LESR signals.

(ii) The higher-energy optical excitation (Hg lamp) also creates another type of paramagnetic center.

(iii) Based on the LDF calculation, optically selective bond scissorings are theoretically expected to be caused in PSi by tuning the excited photon energy. The lowest optical absorption causes the Si skeleton-bond stretching forces, which create WB's. Additional higher optical ab-

sorption causes the Si-pendant dissociating forces, which create DB's.

(iv) The WB produces localized tail states. Excited σ electrons are self-trapped more easily than the excited hole by this WB's tail states, and those electrons and holes are spatially separated.

(v) Accordingly, the LESR signal due to lower-energy excitation is caused by excited σ electrons trapped at the

WB.

(vi) In P*Si*, sodium impurities included in the synthesis process are expected to play an important role in the photo creation of metastable states of P*Si*, similarly to hydrogen in *a*-Si:H. The interaction between these interchain sodium impurities and the paramagnetic state caused by the higher-energy excitation would produce the hyperfine quartet.

*Present address: Electrotechnical Laboratory, Tsukuba 305, Japan.

†Present address: Faculty of Engineering, Yamaguchi University, Ube 755, Japan.

¹R. West, *J. Organomet. Chem.* **300**, 327 (1986).

²R. D. Miller and J. Michl, *Chem. Rev.* **89**, 1359 (1989).

³R. G. Kepler, J. M. Ziegler, L. A. Harrah, and S. R. Kurtz, *Phys. Rev. B* **35**, 2818 (1987).

⁴M. Fujino, *Chem. Phys. Lett.* **136**, 451 (1987).

⁵M. Abkowitz, F. E. Knier, H.-J. Yuh, R. J. Weagley, and M. Stolka, *Solid State Commun.* **62**, 547 (1987).

⁶T. Kagawa, M. Fujino, K. Takeda, and N. Matsumoto, *Solid State Commun.* **57**, 635 (1986).

⁷F. Kajzar, J. Messier, and C. Rosilio, *J. Appl. Phys.* **60**, 3040 (1986).

⁸H. Tachibana, Y. Kawabata, S. Koshihara, and Y. Tokura, *Solid State Commun.* **75**, 5 (1990).

⁹O. Ito, M. Terajima, and T. Azumi, *J. Am. Chem. Soc.* **112**, 444 (1990).

¹⁰W. B. Pollard and G. Lucovsky, *Phys. Rev. B* **26**, 3172 (1982).

¹¹W. L. Wilson and T. W. Weidman, *Mol. Cryst. Liq. Cryst.* **194**, 85 (1991); *J. Phys. Chem.* **95**, 4568 (1991).

¹²P. C. Taylor, in *Semiconductor and Semimetals* edited by J. I. Pankove (Academic, New York, 1984), Vol. 21, Part C. p. 99.

¹³K. Morigaki, *Jpn. J. Appl. Phys.* **28**, L2128 (1989), **29**, L1582 (1990); *J. Non-Cryst. Solids* **141**, 166 (1992).

¹⁴K. Takeda and K. Shiraishi, *Phys. Rev. B* **39**, 11 028 (1990).

¹⁵R. V. Todesco and P. V. Kamat, *Macromolecules* **19**, 196 (1986).

¹⁶A. J. McKinley, T. Karatsu, G. M. Wallraff, R. D. Miller, R. Sooriyakumaran, and J. Michl, *Organometallics* **7**, 2567 (1988).

¹⁷A. J. McKinley, T. Karatsu, G. M. Wallraff, D. P. Thompson, R. D. Miller, and J. Michl; *J. Am. Chem. Soc.* **113**, 2003 (1991).

¹⁸R. E. Benfield, R. H. Cragg, R. G. Jones, and A. C. Swain, *Nature* **353**, 26 (1991).

¹⁹Numerically, the value of 2.0044 is close to that of a dangling bond in the $(\text{SiH}_2)_n$ polysilane alloy part of *a*-Si:H prepared by glow-discharge decomposition of Si_2H_6 . M. Yoshida, K. Morigaki, and S. Nitta, *Solid State Commun.* **51**, 1 (1984).

²⁰Taking account of the molecular weight of P*Si* (~ 100 per Si unit) and the value of the absorption coefficient for the σ - σ^* transition ($\sim 10^4 \text{ cm}^{-1}$), one net LESR centers is distributed in each rod of 10–100 Si skeleton atoms.

²¹In methylpropylpolysilane, the appearance of the same additional structure in the higher-energy excitation was confirmed. The *g* value and that of ΔH_{pp} are the same as

that of dihexypolysilane. Experiments with methylpropylpolysilane higher-energy excitation were not carried out in the present work, but will be reported later.

²²P. Hohenberg and W. Kohn, *Phys. Rev. B* **136**, 864 (1964).

²³W. Kohn and L. J. Sham, *Phys. Rev. A* **140**, 1133 (1965).

²⁴D. R. Hamann, M. Schuler, and C. Chiang, *Phys. Rev. Lett.* **43**, 1494 (1979).

²⁵G. B. Bachelet, D. R. Hamann, and M. Schluter, *Phys. Rev. B* **26**, 4199 (1982).

²⁶D. M. Ceperley and B. J. Alder, *Phys. Rev. Lett.* **45**, 566 (1980).

²⁷J. P. Perdew and A. Zunger, *Phys. Rev. B* **23**, 5048 (1981).

²⁸K. Takeda and K. Shiraishi, *Philos. Mag.* **65**, 535 (1992).

²⁹J. W. Mintmire, *Phys. Rev. B* **39**, 13 350 (1989).

³⁰For a simplicity, we used the parent P*Si*, which has transparent (TP) ideal SiH_2 units, in the following calculation. The essential electronic structure, however, can be discussed by using the parent P*Si* (Ref. 14).

³¹The *x* axis settles along the main axis of the polysilane, and the zigzag skeleton is placed in the *x-y* plane.

³²This "effective" electron trapping has also been reported for the transport properties in P*Si* (Refs. 3–5).

³³Polaron states already have been predicted by M. J. Rice and S. R. Phillpot, *Phys. Rev. Lett.* **58**, 937 (1987).

³⁴A. Tilgner, H. P. Trommsdorff, J. M. Zeigler, and R. M. Hochstrasser, *J. Chem. Phys.* **96**, 781 (1992).

³⁵A. Elschner, R. F. Mahrt, L. Pautmeier, H. Bässler, M. Stolka, and K. McGrane, *Chem. Phys.* **150**, 81 (1991).

³⁶K. A. Klingensmith, J. W. Dowing, R. D. Miller, and J. Michl, *J. Am. Chem. Soc.* **108**, 7438 (1986).

³⁷J. R. G. Thorne, S. T. Repinec, S. A. Abrash, J. M. Zeigler, and R. M. Hochstrasser, *Chem. Phys.* **146**, 315 (1990).

³⁸N. Ishii and T. Shimizu, *Phys. Rev. B* **42**, 9697 (1990).

³⁹M. Cook and C. T. White, *Phys. Rev. Lett.* **59**, 1741 (1987); *Phys. Rev. B* **38**, 9674 (1988).

⁴⁰The elemental analysis for heavy metals (the inductively coupled plasma method) also confirmed that the hyperfine structure by heavy metal impurities, e.g., Mn ($I = \frac{5}{2}$), can be ruled out in the present work, because heavy metal impurities are not included both in nonpurified and purified samples. Chlorine is also a candidate because of its nucleus spin, ($I = \frac{3}{2}$) but is considered to be fully dechloridized by the excess sodium fragments.

⁴¹B. A. Goodman and J. B. Raynar, *Electron Spin Resonance of Transition Metal Complexes*, Advances in Inorganic Chemistry and Radio Chemistry, edited by H. J. Emeleus and A. G. Sharke (Academic, New York, 1970), Vol. 13.